Available online at www.sciencedirect.com
SCIENCE DIRECT®
Journal of Chromatography A, 1069 (2005) 43–52
JOURNAL OF CHROMATOGRAPHY A
www.elsevier.com/locate/chroma

Properties and performance of novel high-resolution/high-permeability ion-exchange media for protein chromatography

Cristina Martin, Jennifer Coyne, Giorgio Carta*

Department of Chemical Engineering, University of Virginia, P.O. Box 400741, Charlottesville, VA 22904-4741, USA

Available online 17 September 2004

Abstract

There is continued interest in the development of stationary phases for protein chromatography that can provide high resolution at elevated flow rates of the mobile phase. When using porous particles, resolution and dynamic binding capacity decline rapidly as the flow rate is increased. Monolithic columns have been developed to overcome these limitations. However, there are difficulties in manufacturing homogeneous larger scale monoliths. In this paper we investigate the morphology and performance characteristics of columns based on new ion exchangers obtained by mechanically disrupting continuous beds of acrylamido-based polymeric media. Near colloidal suspensions of loose particles obtained with this procedure can be flow-packed in ordinary chromatography columns resulting in beds of unexpectedly high hydraulic permeability. Columns up to 2.2 cm in diameter were studied with both Q and S functionalized media. The hydraulic permeability and interparticle porosity of these columns were rather high. The permeabilities of the S and Q media were 1.5×10^{-13} and 2.4×10^{-13} m^2, respectively, while the corresponding porosities were 60 and 70%. These porosity values are similar to those of monoliths, suggesting that these particles assemble under flow to give high-porosity bridged structures. The structure of these packed beds was further characterized by embedding small packed columns in resins and obtaining sections for microscopic observation. The sections reveal the presence of small aggregates of non-porous 1–3 μm particles, surrounded by flow channels several micrometers in size. The height equivalent to a theoretical plate under isocratic and gradient elution conditions and the dynamic binding capacity were determined for several proteins and were found to be virtually independent of flow.

Keywords: Protein chromatography; Monoliths; Permeability; Ion exchange

1. Introduction

In recent years, there has been considerable interest in developing stationary phases for protein chromatography operable at high mobile phase flow rates without loss of resolution and dynamic binding capacity. With conventional porous matrices, the process performance is typically limited by the slow intraparticle diffusion of protein molecules. Reducing the particle size is, of course, helpful. However, as particle size is reduced one normally has to balance the increased chromatographic efficiency against the rapidly increasing operating pressure. As recently reviewed by Josic et al. [1] and by Zou et al. [2], various approaches have been introduced to overcome these limitations including large-pore hydraulically permeable particles, where intraparticle convection replaces diffusion, and monolithic or continuous bed structures, where intraparticle transport is eliminated altogether. The advantages of hydraulically permeable particles have been noted by various authors [3–6]. However, since flow within the particles is driven by the column pressure gradient, advantages can typically be realized only at very high mobile phase flow rates and with small particles tightly packed in a column resulting in high operating pressures.

Several authors [7–12] have also noted the advantages of monoliths or continuous beds. These matrices are typically cast directly in a column resulting in a defined particulate or fibrous-like structure intercalated with a continuously connected network of flow-through pores. Examples of monoliths include polymeric matrices based on acrylamido [11,12], methacrylate [13], and styrene polymers [14] as well as silica [10,15]. Because of their structured characteristics,

* Corresponding author. Tel.: +1 434 924 6281; fax: +1 434 982 2658.
E-mail address: gc@virginia.edu (G. Carta).

0021-9673/$ – see front matter © 2004 Elsevier B.V. All rights reserved.
doi:10.1016/j.chroma.2004.08.114

monoliths generally have greater porosity than equivalent beds formed by randomly packing granular media. Moreover, since the diffusional distances are much smaller than in ordinary chromatographic particles, mass transfer limitations are virtually eliminated resulting in flow-independent resolution and dynamic binding capacity. There are some limitations, however. On the one hand, typical monoliths have a very low permeability compared to ordinary large diameter chromatography particles. For example, based on measurements by Hahn and Jungbauer [7], the permeability of CIM disks (Bia Separations, Ljubljana, Slovenia) is around 0.7×10^{-14} m^2. Such a value results in pressures around 600 bar/m for columns operated at 150 cm/h requiring very short bed depths. On the other hand, monolith columns are often difficult or expensive to manufacture on a larger scale.

1.1. Pressure drop relationships

The pressure drop ($\Delta p/L$) in a packed bed can typically be described by Darcy's law:

$$\frac{\Delta p}{L} = \frac{u\mu}{B_0} \tag{1}$$

where u is the superficial velocity, μ is the mobile phase viscosity, and B_0 is the hydraulic permeability. The latter is in turn related to the particle size, d_p, and the interparticle porosity, ε_b. A common purely empirical relationship is the Giddings equation [16]:

$$B_0 = \frac{\varepsilon_b}{2\phi'} d_p^2 \tag{2}$$

where ϕ' is a flow resistance parameter. According to Giddings, $\phi' = 300 \pm 50$. A second commonly used relationship is the Blake–Kozeny equation [17]:

$$B_0 = \frac{1}{150} \frac{\varepsilon_b^3}{(1-\varepsilon_b)^2} d_p^2 \tag{3}$$

This relationship is semiempirical with the numerical coefficient of 150 adjusted to match a broad range of experimental data. Because of the empirical nature, this equation is valid only over the range of porosities typically encountered in ordinary randomly packed beds. Another relationship is the Happel equation [18]:

$$B_0 = \frac{1}{18\gamma^3} \frac{2 - 3\gamma + 3\gamma^5 - 2\gamma^6}{(2 + 4\gamma^5)/3} d_p^2 \tag{4}$$

where $\gamma = (1-\varepsilon_b)^{1/3}$. The Happel equation is based on a free-surface cell model and is valid, in theory, over a broad range of porosity from the small values found in packed beds to those of swarms of isolated particles. Finally, a fourth relevant relationship is the Jackson and James equation [19] for three-dimensional arrays of fibers with $\varepsilon_b \geq 0.7$:

$$B_0 = \frac{3}{80\gamma^3}(-\ln \gamma^3 - 0.931) d_p^2 \tag{5}$$

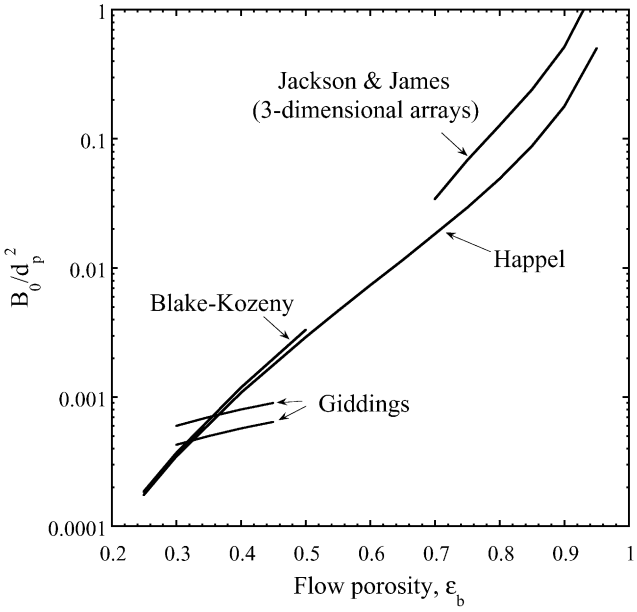

Fig. 1. Effect of interparticle porosity on specific permeability predicted from various models.

A comparison of these equations plotted over their range of approximate validity is shown in Fig. 1. There is a fair agreement between the Blake–Kozeny and the Happel equation and a relatively small difference (less than a factor of 2) between Happel and the Jackson and James equation. All these relationships show a strong dependence of hydraulic permeability on porosity, which explains the relative success of monoliths or continuous beds. The Giddings equation provides values similar to the Blake–Kozeny in the range of typical packed-bed porosities (0.35–0.45).

In this paper we report the properties of new chromatographic matrices obtained from Bio-Rad Labs. (Hercules, CA, USA) that, surprisingly, while consisting of loose particles, result in stable packed bed interparticle porosities in the range 0.60–0.70. As seen in Fig. 1, values of ε_b in this range should result in specific permeabilities (B_0/d_p^2) that are much higher than those expected for ordinary columns. Because of the relatively high permeability, these matrices allow operation at relatively small pressures and with small particle sizes resulting in flow-independent resolution and dynamic binding capacity for proteins.

2. Materials and methods

2.1. Materials

UNOPlus Q and UNOPlus S stationary phases were obtained from Bio-Rad Labs. (Hercules, CA, USA) with quaternary ammonium ion (Q) and sulphopropyl (S) functionality, respectively. According to the manufacturer, these matrices are produced by first polymerizing acrylamido

and vinyl monomers to form a continuous bed matrix in a manner similar to that described in [12]. The matrix is then mechanically disrupted by ultrasonication to obtain free-flowing, loose particles that can be packed in ordinary medium-pressure chromatography columns. Chromatographic columns made by disrupting and reconstituting continuous bed matrices have been described previously by Hjertén et al. [20,21]. The disrupted media was described as consisting of large lumps, 1–2 mm in size, consisting of aggregates of small particles. These columns were highly compressed and resulted in relatively low permeabilities. However, the UNOPlus matrices considered in this work appear different. They consist of small individual particles that can be flow-packed to form stable beds without high bed compression. UNOSphere S particles (originally introduced in [22] as BRX-S) were also used as a control in our microscopy studies. This media has substantially the same chemistry as UNOPlus but it comprises porous spheroidal particles approximately 63 μm in diameter [22].

Bovine serum albumin, α-lactalbumin, ovalbumin, cytochrome *c*, lysozyme, and α-chymotrypsinogen were obtained from Sigma (St. Louis, MO, USA). IgG was obtained from Pharmacia (St. Louis, MO, USA). Chemicals for the preparation of embedding media for TEM imaging (Spurr's Low Viscosity Embedding Mixture, catalog No. 14300) were from Electron Microscopy Sciences (Ft. Washington, PA, USA). Other chemicals were obtained from Sigma and from Fisher Scientific (Pittsburgh, PA, USA). All experiments were conducted at room temperature (T = 22 ± 2 °C). A 25 mM Tris–HCl buffer at pH 8.5 was used for runs with UNOPlus Q. Either a 10 mM Na_2HPO_4 buffer at pH 6.5 (for most proteins) or a 20 mM CH_3COONa pH 5.0 buffer (for IgG) was used for runs with UNOPlus S.

2.2. Microscopy

Morphological features of the packed media were studied by microscopy. For this purpose small packed beds were embedded in a resin matrix using procedures similar to that in [22]. Small disposable columns (0.5 cm diameter) were packed with the particles at 500 cm/h. The columns were then dehydrated by passing an ethanol–water (50:50, v/v) mixture followed by several volumes of anhydrous ethanol. A Spurr's embedding media containing 10 g of vinylcyclohexene dioxide, 4 g of diglicidyl ether of polypropylene glycol, 26 g of nonenyl succinic anhydride and 0.3 g of dimethylaminoethanol was prepared. The dehydrated columns were then perfused with several volumes of an ethanol–Spurr's resin (50:50, v/v) mixture followed by several volumes of pure Spurr's resin. The resin-infiltrated columns were then cured overnight at 70 °C and sectioned in 1 μm slices for optical microscopy and in 70 nm sections for TEM using a Leica Ultracut UCT microtome equipped with a Diatome diamond knife (45°). The sections were stained with a 2% aqueous uranyl-lead acetate solution. TEM analyses were done with a JEOL 100 CX electron microscope.

2.3. Isocratic and gradient elution chromatography

Isocratic elution (IE) and linear gradient elution (LGE) chromatography experiments were conducted by packing a 50:50 slurry of the media in distilled water under flow at 500 cm/h in 10 cm × 1 cm glass columns (model HR10/10, Amersham Biosciences, Piscataway, NJ, USA). The columns were equilibrated at 500 cm/h with an additional 5–10% plunger compression, resulting in final bed heights of 9 ± 0.5 cm. IE experiments were done at high salt concentrations (1 M NaCl) for conditions of no retention while LGE experiments were done with NaCl gradients from 0 to 500 or 750 mM. A BioLogic DuoFlow system from Bio-Rad Labs. was used at flow rates of 0.5–6 mL/min with UV detection at 280 nm. A Waters refractive index detector was used for experiments with dextran T-500. A limited number of isocratic elution experiments aimed at testing packing reproducibility were also done in 0.5 cm diameter columns (model HR5/5, Amersham Biosciences) and in 2.2 cm diameter columns (Model Vantage-L, Millipore, Bedford, MA, USA). These columns were packed as indicated above with final bed heights of 5 ± 0.5 cm. Experiments with the 2.2 cm columns were conducted with a ProSys unit (BioSepra, Marlborough, MA, USA) at flow rates up to 30 mL/min.

Hydraulic permeabilities were determined from pressure flow curves after subtracting the system pressure. Retention volumes and height equivalent to a theoretical plate (HETP) values were determined either using the moment method or graphically. In either case, extracolumn contributions to the retention volume and the peak variance were subtracted from the raw data based on pulse injections made with empty columns having the column inlet and outlet distributors pushed together. Finally, retention factors as a function of salt concentration and HETP as a function of flow rate were determined for the LGE experiments based on the procedure of Yamamoto [23].

2.4. Frontal analysis

Breakthrough experiments were done in 0.5 cm diameter glass columns (model HR5/5, Amersham Biosciences) packed as previously described. Buffered solutions containing 1 mg/mL protein were fed to the column using a LabAlliance (State College, PA, USA) Series II pump at flow rates up to 500 cm/h. Breakthrough curves were monitored through the Biologic DuoFlow UV detector at 280 nm. After each run, the UNOPlus Q and the UNOPlus S columns were desorbed with 500 mM NaCl and 750 mM NaCl, respectively, requilibrated in buffer and reused.

3. Results and discussion

Fig. 2 shows optical microscopy images of 1 μm sections of embedded UNOPlus Q and S and UNOSphere S columns. The light gray areas represent the embedding resin while the darker regions are the stained matrix material. It can be seen

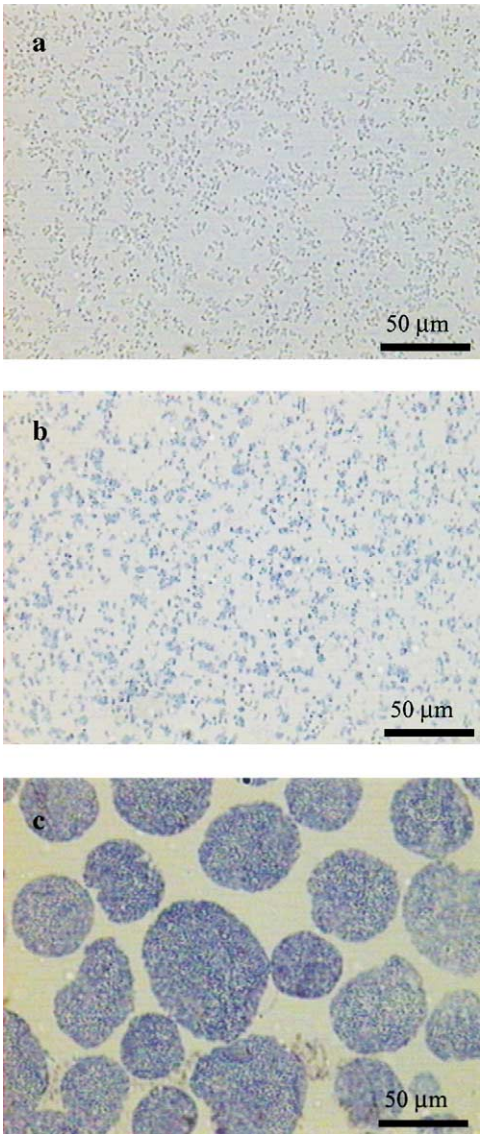

Fig. 2. Optical microscopy of packed bed sections of (a) UNOPlus Q; (b) UNOPlus S; and (c) UNOSphere S.

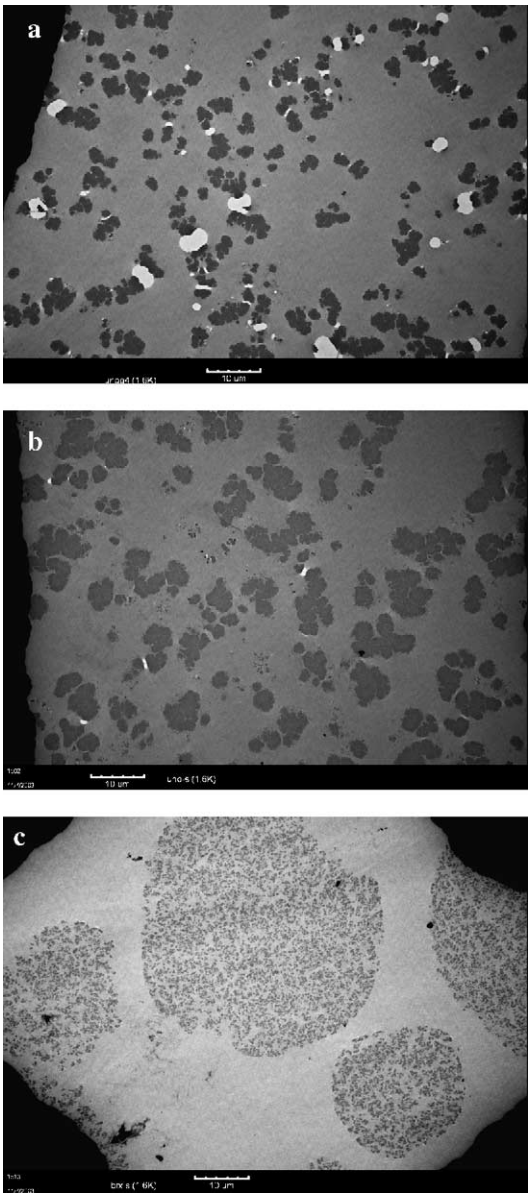

Fig. 3. Transmission electron micrographs of packed bed sections of (a) UNOPlus Q; (b) UNOPlus S; and (c) UNOSphere S. The white bar scale is 10 μm.

that the UNOSphere S media particles are closely packed. Interestingly, the internal macroporous structure of the particles is also visible, although the pores are likely too small to allow convective flow. As a result, the flow is normally confined to the interparticle space. In the case of UNOPlus Q and UNOPlus S, the particles are much smaller and appear to be considerably further apart. This is more evident in the higher magnification TEM images in Figs. 3 and 4. It can be seen that the UNOPlus media define relatively large flow channels. The media appear to be comprised of 1–3 μm nodules that are aggregated to a certain extent. Interestingly, this result is very close to the scanning electron micrographs obtained by Garke et al. [9] for UNO columns. These authors have reported that a structure consisting of 2–3 μm interconnected non-porous nodules exists in UNO continuous bed columns. Apparently, a similar structure and a high interparticle porosity is also established when the UNOPlus particles are flow-packed in a column. Fig. 4 shows that the nodules in UNOPlus are also non-porous, although they appear to have substantial surface roughness.

Column porosities were calculated from the retention volume of dextran tracers (Blue dextran, M_r = 2 000 000, for UNOPlus S and dextran T-500, $M_r \sim$ 500 000, for UNOPlus Q) and for different proteins under conditions of no retention. Calculated porosities are summarized in Table 1. It can be seen that for the macromolecules there is very little difference in accessible porosity in spite of the broad size range of the different solutes. Since, as seen from the TEM images, the UNOPlus particles are non-porous or contain only very small pores, the porosity determined from the retention

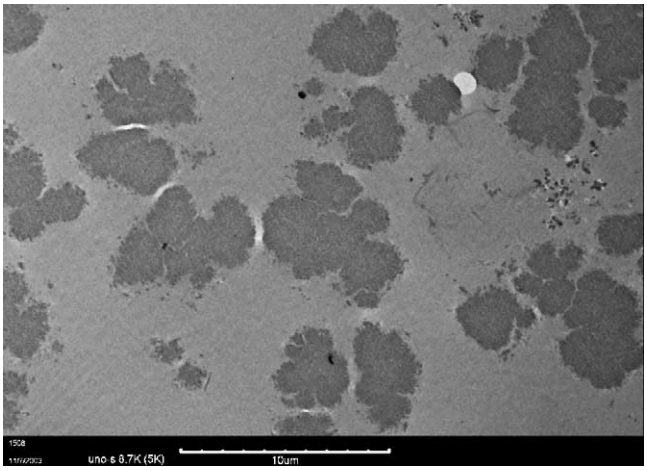

Fig. 4. High magnification transmission electron micrograph of a packed bed section of UNOPlus S.

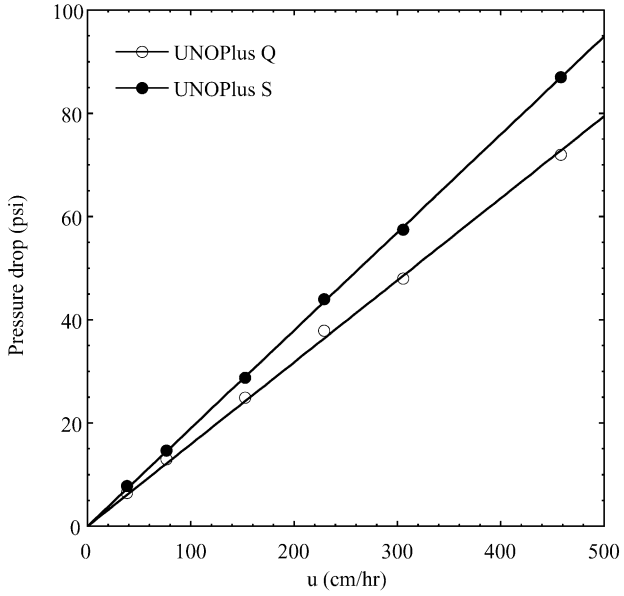

Fig. 5. Pressure flow curves for 9 cm × 1 cm UNOPlus Q and UNOPlus S columns after subtracting the system pressure.

volume is interparticle. Porosity values are somewhat higher for UNOPlus Q, which appears to be consistent with the TEM images. As seen in Table 1, acetone behaves in a manner different from the various macromolecules tested yielding a larger retention volume. It is likely that this small solute diffuses in the solid polymer matrix giving the impression of a greater total porosity. Obviously, the apparent porosity measured by the acetone retention volume is not available for fluid flow.

Fig. 5 shows the pressure-flow curves for the 1-cm diameter columns. The curves are linear over the entire range of flow rates and similar results were obtained for 0.5 and 2.2 cm diameter columns. The corresponding permeability values are shown in Table 2 in comparison with values for various commercial monoliths. As suggested by Hahn and Jungbauer [7], an equivalent particle size based on the permeability and porosity values can be calculated using an appropriate permeability relationship. In our case, the Happel equation was used, since this equation seems appropriate for the range of porosities observed. The results are shown in Table 2. The calculated d_p values appear to be consistent with the actual particle sizes observed microscopically for UNOPlus media suggesting that the Happel equation captures the flow characteristics along with the porosity values determined from pulse injection experiments. This conclusion also appears to be valid for various monoliths. For example, as reported by Hahn and Jungbauer, the BIA CIM disks have actual particle sizes in the 1–2 μm range, consistent with the value calculated from hydraulic permeability and porosity. As seen in Table 2, the UNOPlus permeability values are significantly higher than those of several monoliths.

The effect of flow rate on the isocratic elution behavior of several proteins under unretained conditions is shown in Fig. 6. It is evident that there is no significant effect of flow rate on either retention volume or bandspreading. As a result, it can be concluded that there are no diffusional limitations. The corresponding HETP values are shown in Fig. 7. These values are quite low compared to ordinary porous chromatography particles, they are essentially independent of flow, and they are the same within experimental error for proteins with vastly different molecular masses. This result is consistent with the absence of diffusional limitations.

LGE experiments for UNOPlus S are shown in Figs. 8 and 9 for mixtures of α-chymotrypsinogen and

Table 1
Column porosity determined from pulse injections for conditions of no retention

UNOPlus Q, ε_b		UNOPlus S, ε_b	
Acetone	0.75	Acetone	0.79
α-Lactalbumin[a]	0.70	Cytochrome *c*[a]	0.64
BSA[a]	0.69	BSA	0.61
Dextran T-500	0.70	IgG[a]	0.60
		Blue dextran	0.60

[a] Measurements in 1 M NaCl.

Table 2
Comparison oorosity, permeability and equivalent particle size for UNOPlus media and monoliths

Media	Data source reference	Porosity, ε_b	Permeability, B_0 ($\times 10^{-14}$ m^2)	Equivalent particle size, d_p (μm)
CIM Disks	[7]	0.50	0.7	1.5
Methacrylate monoliths	[27]	0.62	2.8	1.8
UNO	[12]	ND	2.2–6.0	ND
Silica rods SR-(I)-S	[15]	0.65	10.2	2.9
SilicaROD	[10]	ND	6.0–12.0	ND
UNOPlus Q	This work	0.69	24.0	3.8
UNOPlus S	This work	0.60	15.0	4.5

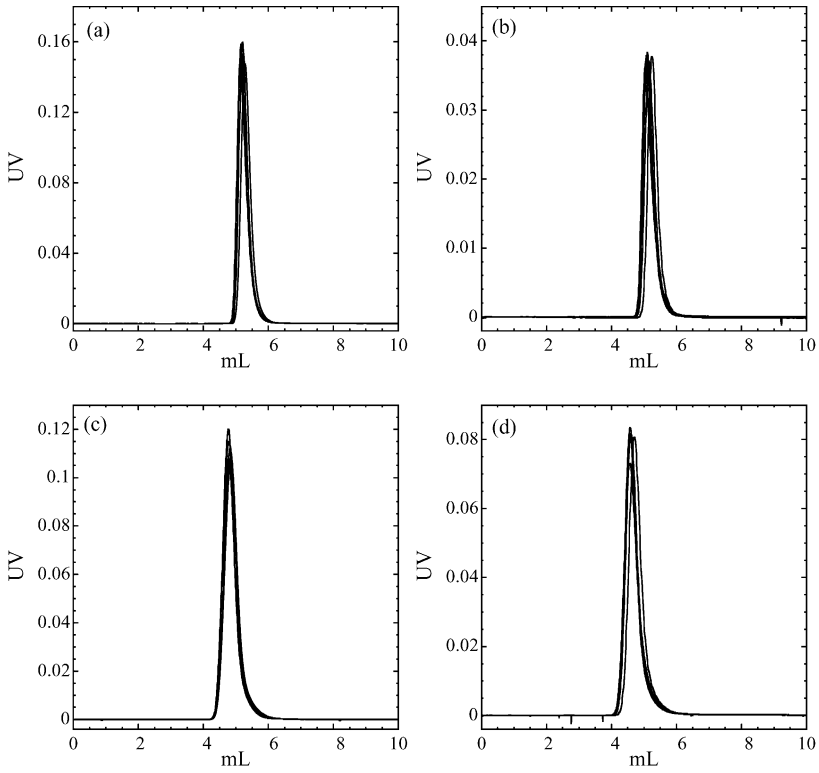

Fig. 6. Pulse injection response of 9 cm × 1 cm UNOPlus Q and UNOPlus S columns at 0.5, 1, 2, 3, and 4 mL/min for conditions of no retention (1 M NaCl): (a) α-lactalbumin on UNOPlus Q; (b) BSA on UNOPlus Q; (c) cytochrome *c* on UNOPlus S; (d) IgG on UNOPlus S.

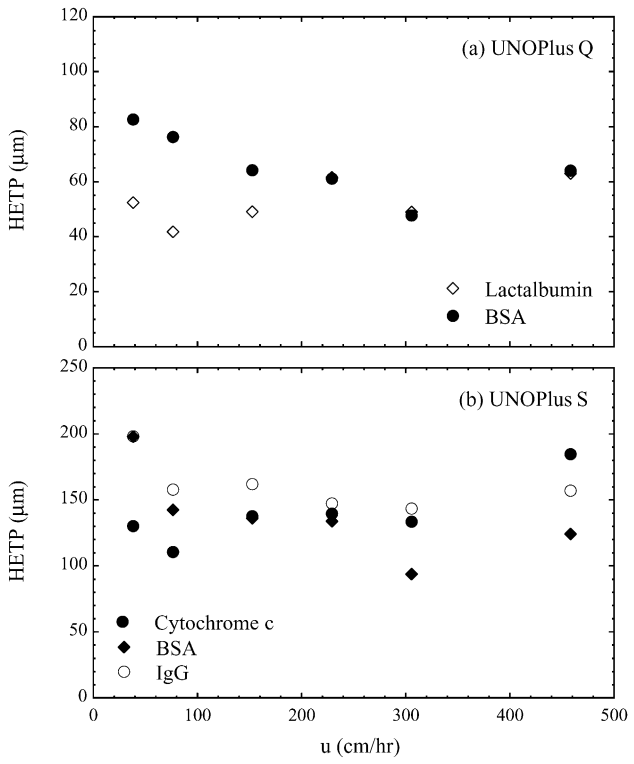

Fig. 7. HETP calculated from pulse injection response of 9 cm × 1 cm UNOPlus Q (a) and UNOPlus S (b) columns for conditions of no retention (1 M NaCl).

lysozyme. Fig. 8 shows the effect of gradient volume at constant flow rate, while Fig. 9 shows the effect of flow rate with a constant gradient volume. It can be seen that the separation is completely independent of flow rate. Impurities present in the protein samples are also resolved resulting in additional peaks. The effect of sample load is shown in Fig. 10. There is no apparent change in resolution and retention time.

Retention factor and HETP were obtained for the LGE runs using the method of Yamamoto [23]. Briefly, the retention factor, k', is expressed as a function of salt concentration, C_M, according to:

$$k' = AC_M^{-z} \tag{6}$$

where A is an equilibrium parameter and z is the effective charge. For linear gradient elution, the following relationship exists between gradient volume, V_G, and the salt concentration at which the peak elutes, C_M^R [24]:

$$\gamma = \frac{V_0\,\Delta C_M}{V_G} = \frac{1}{A(z+1)}[(C_M^R)^{(z+1)} - (C_M^0)^{(z+1)}] \tag{7}$$

where V_0 is the column void volume and ΔC_M the salt concentration change. Since the term $(C_M^0)^{z+1}$ is typically very small, A and z can be determined by linear regression of $\log(\gamma)$ versus $\log(C_M^R)$ for experiments where V_G is varied.

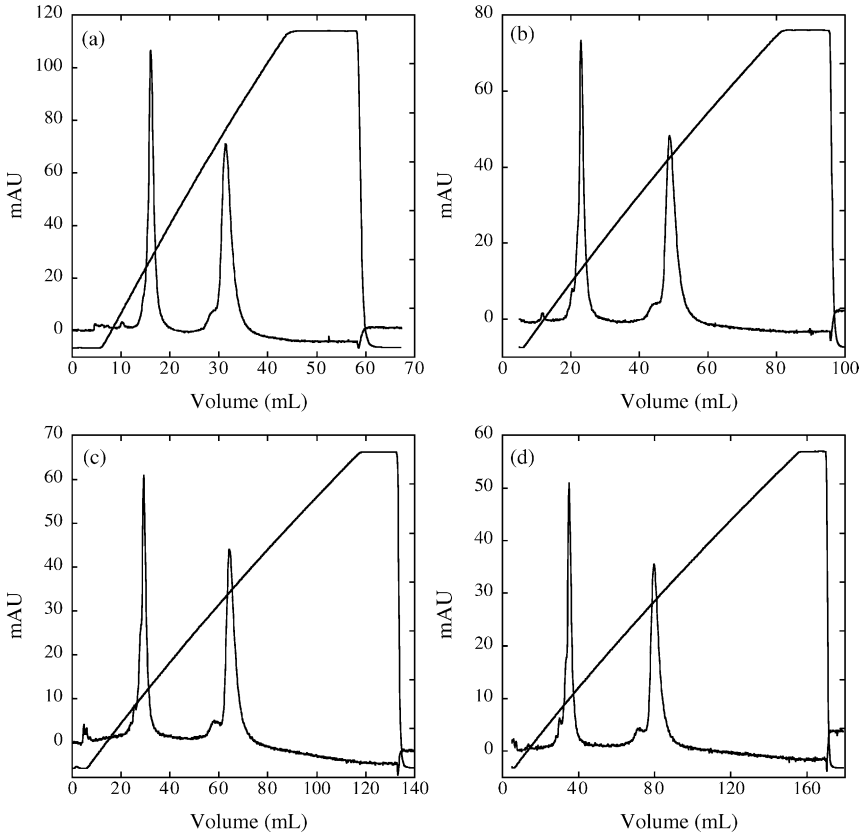

Fig. 8. LGE separation of α-chymotrypsinogen/lysozyme mixture in 9 cm × 1 cm UNOPlus S columns at 2 mL/min with 0–750 mM NaCl gradient with different gradient duration: (a) 5 CV gradient; (b) 10 CV gradient; (c) 15 CV gradient; (d) 20 CV gradient.

Following Yamamoto [23], the HETP can be calculated from the equation:

$$\mathrm{HETP} = \frac{1}{16}\frac{W^2 L}{V_R^2}\frac{1}{\ell^2} \quad (8)$$

where W is the peak baseline width, $V_R = V_0[1 + k'(C_M^R)]$ is the retention volume calculated at $C_M = C_M^R$, and ℓ is a correction factor that depends on the parameter $M = [1 + k'(C_M^R)](z + 1)/(1 + k'_M)z$. k'_M is the retention factor for the

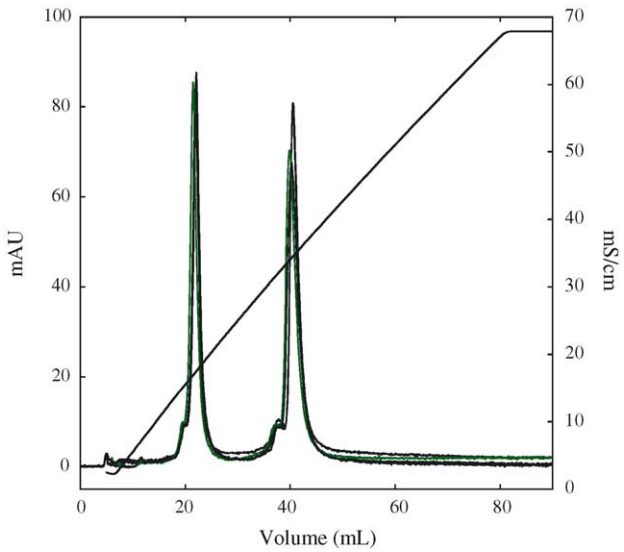

Fig. 9. LGE separation of α-chymotrypsinogen/lysozyme mixture in 9 cm × 1 cm UNOPlus S column with 0–750 mM NaCl gradient in 10 CV at flow rates of 0.5, 1, 2, and 4 mL/min.

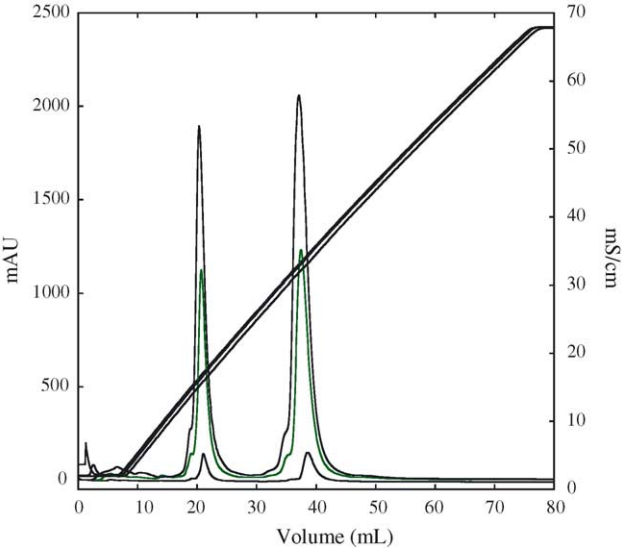

Fig. 10. LGE separation of α-chymotrypsinogen/lysozyme mixture in 9 cm × 1 cm UNOPlus S column with 0–750 mM NaCl gradient in 10 CV and flow rate of 2 mL/min with protein loads of 1, 5, and 10 mg.

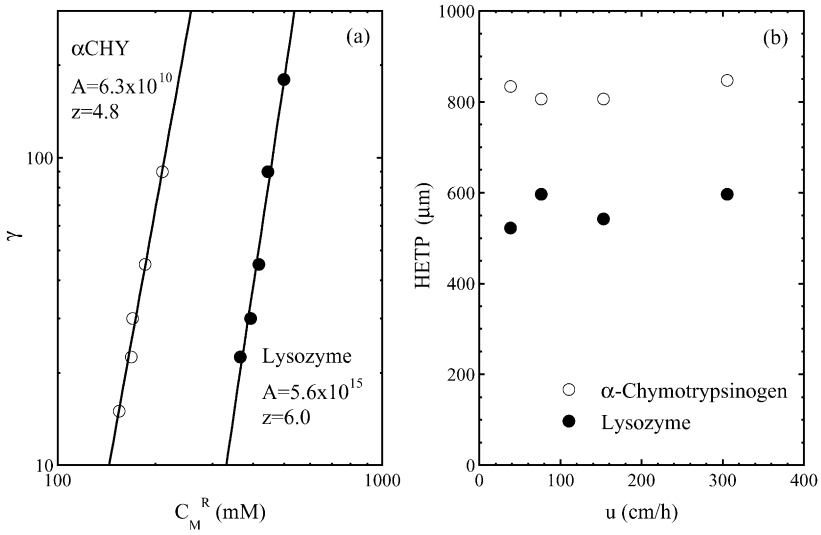

Fig. 11. Calculated parameter values based on LGE separation of α-chymotrypsinogen/lysozyme mixture in 9 cm × 1 cm UNOPlus S column: (a) retention factor parameters; (b) HETP.

salt, which is essentially zero in our case. Expressions for ℓ are given in [23]. The results of these calculations are shown in Fig. 11. The z-values obtained from Fig. 11a are typical for proteins of this size. However, the HETP values are higher than those obtained under conditions of no retention. Ideally, HETP values obtained from gradient elution according to the method of Yamamoto should be comparable to those obtained under isocratic elution conditions since this approach is designed to provide the corrections needed to make the comparison possible. However, as seen by comparison of our isocratic and LGE results, this was not the case for our high performance matrix. We suspect that this occurred because of the approximate nature of the Yamamoto approach that does not account for non-linearities in the early stages of the gradient elution process and for the ensuing thermodynamic bandspreading effects. These effects may not be important for a low efficiency column, but may become quite significant for our high-resolution matrix. More importantly, however, the HETP values derived from the LGE results are also independent of flow rate confirming the absence of kinetic or diffusional limitations even under separation conditions. Similar results were obtained for UNOPlus Q. An example is given in Fig. 12 showing the separation of α-lactalbumin/BSA mixtures. The separation is again nearly completely independent of flow rate. The small late eluting peak is likely a BSA dimer.

Breakthrough curves for different proteins with UNOPlus Q and S columns are shown in Fig. 13. It can be seen that the curves are independent of flow rate, a result that is again consistent with the absence of diffusional or kinetic limitations. As seen in Fig. 13b, the BSA breakthrough curve is very steep up to $C/C_F \sim 0.9$ and gradual thereafter. This behavior has been attributed to the competitive binding of a BSA dimer that is present in these samples (cf. Fig. 12 and [25]). It is possible that a similar factor contributes to the tailing behavior of IgG seen in Fig. 13d. Finally, the dynamic binding capacity (DBC) at $C/C_F = 0.1$ is shown in Fig. 14. The DBC values are slightly different for the different protein, but this can be expected, since the static capacity is also different. However, the DBC is in all cases completely independent of flow rate. It should be noted that the dynamic binding capacities found in this work are substantially lower than those observed for many chromatography matrices based on porous particles or gels. However, they are similar to DBC values that have been reported for various monoliths. For example, Iberer et al. [8] have reported BSA binding capacities in the range of 20–30 mg/mL for CIM-QA Disks and UNO-Q monoliths while Hahn et al. [26] have reported capacities in the 20–30 mg/mL for lysozyme and IgG on CIM-S disks.

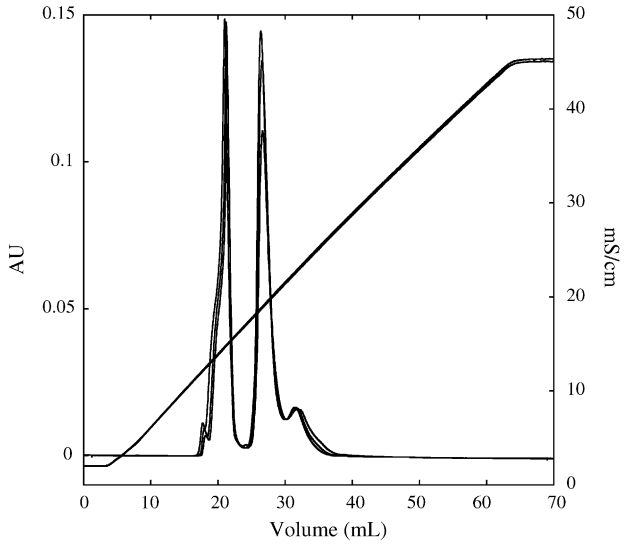

Fig. 12. LGE separation of α-lactalbumin/BSA mixture in 9 cm × 1 cm UNOPlus Q column with 0–500 mM NaCl gradient in 8.7 CV at flow rates of 0.5, 2, and 6 mL/min.

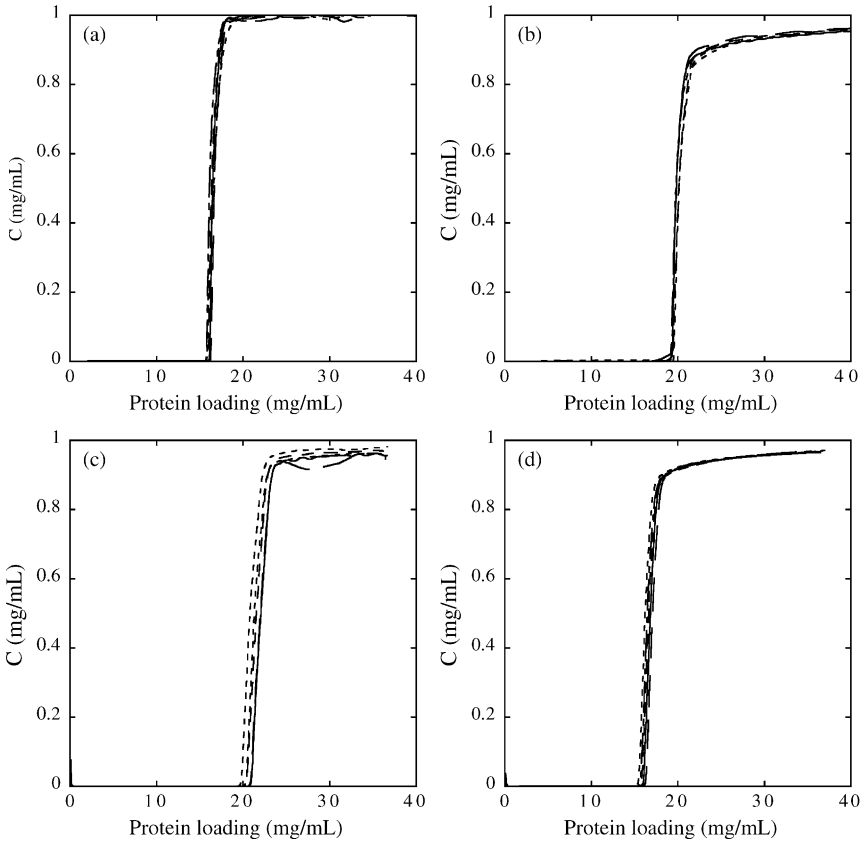

Fig. 13. Breakthrough curves for 5 cm × 0.5 cm UNOPlus Q and UNOPlus S columns at 0.12, 025, 0.5, 0.75, 1, and 1.5 mL/min (37–458 cm/h) with 1 mg/mL protein solutions: (a) α-lactalbumin on UNOPlus Q; (b) BSA on UNOPlus Q; (c) lysozyme on UNOPlus S; (d) IgG on UNOPlus S.

A final consideration is the reproducibility of packing at different scales. Pulse injection experiments were done with α-lactalbumin and BSA in 1 M NaCl with UNOPlus Q and with BSA and Blue Dextran with UNOPlus S using columns 0.5 and 2.2 cm in diameter. The results are shown in Table 3. It can be seen that the porosity values determined from the retention volumes for these unretained probes are practically independent of scale. Permeabilities were also quite similar

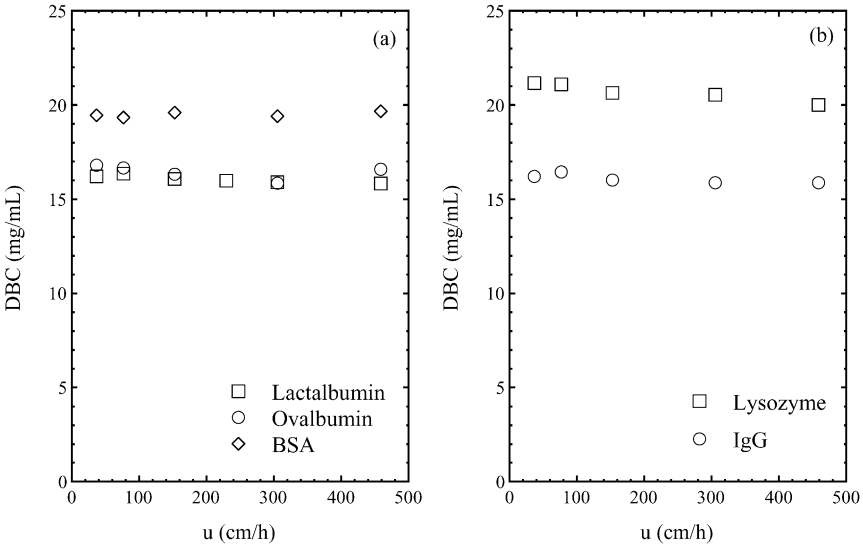

Fig. 14. Dynamic binding capacity for 5 cm × 0.5 cm (a) UNOPlus Q and (b) UNOPlus S columns at 10% of breakthrough.

Table 3
Comparison of porosities for UNOPlus columns with different diameters determined from pulse injections of lactalbumin and BSA in 1 M NaCl for UNOPlus Q and BSA and blue dextran for UNOPlus S

Column diameter (cm)	UNOPlus Q, ε_b	UNOPlus S, ε_b
0.5	0.61	0.62
1.0	0.69	0.60
2.2	0.68	0.59

and there was no effect of flow rate on peak shape and retention volume.

4. Conclusions

We have demonstrated that UNOPlus media can be packed reproducibly in medium-pressure chromatography columns resulting in beds with very high void fraction and relatively high hydraulic permeability. The particles are non-porous and are 1–3 μm in size. They have, however, a rough surface. As a result of the small size of these particles and the absence of intraparticle pores, flow-independent resolution and dynamic binding capacities are obtained even for high-molecular-mass proteins. High-resolution separations can be obtained in gradient elution using ordinary equipment. The reasons for the surprisingly high interparticle porosities are not known. Perhaps the surface roughness and the near colloidal properties of the loose particles result in the formation of bridged structures that define open flow channels when the column is packed under flow. As a result, beds of considerable permeability are obtained with performance characteristics that resemble those of commercial monoliths formed in place within the column.

Acknowledgment

This research was supported by Bio-Rad Laboratories.

References

[1] D. Josic, A. Buchacher, A. Jungbauer, J. Chromatogr. B 752 (2001) 191.
[2] H. Zou, X. Huang, M. Yie, Q. Luo, J. Chromatogr. A 954 (2002) 5.
[3] N.B. Afeyan, N.F. Gordon, I. Mazsaroff, L. Varady, S.P. Fulton, Y.B. Yang, F.E. Regnier, J. Chromatogr. 519 (1990) 1.
[4] G. Carta, M.E. Gregory, D.J. Kirwan, H.A. Massaldi, Sep. Technol. 2 (1992) 62.
[5] G. Carta, A.I. Rodrigues, Chem. Eng. Sci. 48 (1993) 3927.
[6] A.I. Liapis, M.A. McCoy, J. Chromatogr. 599 (1992) 87.
[7] R. Hahn, A. Jungbauer, Anal. Chem. 72 (2000) 4853.
[8] G. Iberer, R. Hahn, A. Jungbauer, LC GC 17 (1999) 1000.
[9] G. Garke, I. Radtschenko, F.B. Anspach, J. Chromatogr. A 857 (1999) 137.
[10] B. Bidlingmaier, K.K. Unger, N. Von Doehren, J. Chromatogr. A 832 (1999) 11.
[11] S. Hjertén, J.-L. Liao, J. Chromatogr. 458 (1988) 165.
[12] T.L. Tisch, R. Frost, J.-L. Liao, W.-K. Lam, A. Remy, E. Scheinpflug, C. Siebert, H. Song, A. Stapleton, J. Chromatogr. A 816 (1998) 3.
[13] F. Svec, J.M.J. Frechet, J. Chromatogr. A 702 (1995) 89.
[14] Q.C. Wang, F. Svec, J.M.J. Frechet, Anal. Chem. 65 (1993) 2243.
[15] H. Minakuchi, K. Nakanishi, N. Soga, N. Ishizaka, N. Tanaka, J. Chromatogr. A 762 (1997) 135.
[16] J.C. Giddings, Dynamics of Chromatography. Part 1. Principles and Theory, Marcel Dekker, New York, 1965.
[17] R.B. Bird, W.E. Stewart, E.N. Lightfoot, Transport Phenomena, Wiley, New York, 1960.
[18] J. Happel, AIChE J. 4 (1958) 197.
[19] G.W. Jackson, D.F. James, Can. J. Chem. Eng. 64 (1986) 364.
[20] S. Hjertén, J. Mohammad, J.-L. Liao, Biotechnol. Appl. Biochem. 15 (1992) 247.
[21] S. Hjertén, J. Mohammad, K. Nakazato, J. Chromatogr. 646 (1993) 121.
[22] A.K. Hunter, G. Carta, J. Chromatogr. A 897 (2000) 65.
[23] S. Yamamoto, Biotechnol. Bioeng. 48 (1995) 444.
[24] M.D. LeVan, G. Carta, C. Yon, in: D.W. Green (Ed.), Perry's Chemical Engineers' Handbook, 7th ed., McGraw-Hill, New York, 1997. Section 16.
[25] A.K. Hunter, G. Carta, J. Chromatogr. A 937 (2001) 13.
[26] R. Hahn, M. Panzer, E. Hansen, J. Mollerup, A. Jungbauer, Sep. Sci. Technol. 37 (2002) 1545.
[27] D. Sycora, F. Svec, J.M.J. Frechet, J. Chromatogr. A 852 (1999) 297.